J Neuropathol Exp Neurol
Vol. 0, No. 0, 2018, pp. 1–6
doi: 10.1093/jnen/nlx116

OXFORD

BRIEF REPORT

Persistence of Zika Virus After Birth: Clinical, Virological, Neuroimaging, and Neuropathological Documentation in a 5-Month Infant With Congenital Zika Syndrome

Leila Chimelli, MD, PhD, Sheila Moura Pone, MD, PhD, Elyzabeth Avvad-Portari, MD, PhD, Zilton Farias Meira Vasconcelos, PhD, Andrea Araújo Zin, MD, PhD, Daniela Prado Cunha, MS, Nathalia Raposo Thompson, MD, Maria Elisabeth Lopes Moreira, MD, PhD, Clayton A. Wiley, MD, PhD, and Marcos Vinicius da Silva Pone, MD, PhD

Abstract

During the Zika epidemic in Brazil, a baby was born at term with microcephaly and arthrogryposis. The mother had Zika symptoms at 10 weeks of gestation. At 17 weeks, ultrasound showed cerebral malformation and ventriculomegaly. At 24 weeks, the amniotic fluid contained ZIKV RNA and at birth, placenta and maternal blood were also positive using RT-qPCR. At birth the baby urine contained ZIKV RNA, whereas CSF at birth and urine at 17 days did not. Seizures started at 6 days. EEG was abnormal and CT scan showed cerebral atrophy, calcifications, lissencephaly, ventriculomegaly, and cerebellar hypoplasia. Bacterial sepsis at 2 months was treated. A sudden increase in head circumference occurred at 4 months necessitating ventricle-peritoneal shunt placement. At 5 months, the infant died with sepsis due to bacterial meningitis. Neuropathological findings were as severe as some of those found in neonates who died soon after birth, including hydrocephalus, destructive lesions/calcification, gliosis, abnormal neuronal migration, dysmaturation of nerve cells, hypomyelination, loss of descending axons, and spinal motor neurons. ZIKV RNA was detected only in frozen brain tissue using RT-qPCR, but infected cells were not detected by in situ hybridization. Progressive gliosis and microgliosis in the midbrain may have contributed to aqueduct compression and subsequent hydrocephalus. The etiology of progressive disease after in utero infection is not clear and requires investigation.

Key Words: Arthrogryposis, Calcification, Hydrocephalus, Microcephaly, Neuropathology, RT-qPCR, Zika virus.

From the Laboratory of Neuropathology, State Institute of Brain and UFRJ (LC); Pediatric Infectious Diseases (SMP, NRT, MVdSP); Pathology (EA-P); Clinical Research Unit (ZFMV, AAZ, DPC, MELM); National Institute of Women, Children and Adolescents Health Fernandes Figueira (IFF) – Oswaldo Cruz Foundation (Fiocruz), Rio de Janeiro, Brazil; and Division of Neuropathology, UPMC Presbiterian Hospital, Pittsburgh, Pennsylvania (CAW)

Send correspondence to: Leila Chimelli, MD, PhD, Laboratory of Neuropathology, State Institute of Brain, Rua do Resende 156, Centro, Rio de Janeiro, RJ CEP 20231-092, Brazil; E-mail: chimelli@hucff.ufrj.br

The authors have no duality or conflicts of interest to declare.

INTRODUCTION

A major concern associated with Zika virus (ZIKV) infection is the increased incidence of microcephaly in infants born to infected mothers. In addition, early calcification and other malformations including ventriculomegaly, cerebellar hypoplasia, and arthrogryposis are associated with congenital Zika infection (1–3). Individual case reports and case series of autopsies demonstrated ZIKV persistence in fetal and newborn brain tissue, either by reverse transcriptase-quantitative polymerase chain reaction (RT-qPCR), electron microscopy, in situ hybridization (ISH), and/or immunohistochemistry (3–6). The spectrum of neuropathological lesions associated with congenital ZIKV infection in patients who did not survive was defined (5). However, most infants with congenital Zika syndrome are alive, now reaching their second year of life, some with motor deficits, seizures, feeding difficulties, visual or auditory symptoms, in addition to arthrogryposis (2, 7, 8). Persistence of viral infection and progression of the lesions have been a matter of debate among pediatricians and infectious disease physicians (4) and have been investigated experimentally (9). Herein, we report a comprehensive clinical, virological, neuroimaging, and pathological analysis of an infant with congenital ZIKV syndrome, who survived 5 months.

CASE REPORT

During the epidemic of Zika in Brazil, a baby girl was born at term (38 weeks) with microcephaly and arthrogryposis in all 4 limbs. The mother reported Zika symptoms (cutaneous rash, headache, myalgia, and vertigo) at ~10 weeks of gestation. She did not receive medical attention and did not use any medications. At 17 weeks, fetal ultrasound showed cerebral malformation, ventriculomegaly, flexed hands and feet. At 24 weeks and 5 days, amniotic fluid was positive for Zika (by RT-qPCR). Gestation was followed to term with imaging tests always pointing to the same malformations described at 17 weeks. The placenta was sent for pathological analysis. At birth, placenta and mother blood were positive for Zika (by RT-qPCR). The fetal karyotype was normal (46, XX) and

© 2018 American Association of Neuropathologists, Inc. All rights reserved.

maternal STORCH (syphilis, toxoplasmosis, others, rubella, cytomegalovirus, herpes) serologies were negative.

The baby was born with APGAR?/8, weighing 1920 g, head circumference 29 cm, below percentile 5 (10) and length 47 cm, with dyspnea, but no need for resuscitation. STORCH serologies were also negative. There was craniofacial disproportion, umbilical hernia, and bilateral hip instability. She remained in the nursery with impetigo and respiratory symptoms for 35 days and was followed by a multidisciplinary team. The echocardiogram showed interatrial communication, patent *foramen ovale*, pulmonary artery stenosis.

The patient presented with clonic seizures at 6 days, then generalized fits and an electroencephalogram showed generalized multifocal anomalies, predominantly in the right temporal domain. Skull computed tomography (CT) revealed periventricular and diffuse calcifications, including the basal ganglia, lissencephaly, cerebral atrophy, supratentorial ventriculomegaly sparing the fourth ventricle, brainstem and cerebellar hypoplasia (Fig. 1). There was hypertonia of the limbs and important delay of the neuropsychomotor development, optic nerve pallor and macular atrophy in the right eye. Auditory screening was abnormal, but auditory brainstem evoked potential was normal.

At 2 months, she was admitted with sepsis, which was treated. The organism was not known. At 4 months, there was a sudden increase of the head circumference (from 32.5 to 39 cm), bulging of the fontanels and vomiting, when a ventricle-peritoneal shunt was placed. Four days before death (at 5 months), when the head circumference was 40.5 cm, the child was admitted with sepsis due to bacterial meningitis. Three organisms were identified suggesting contamination.

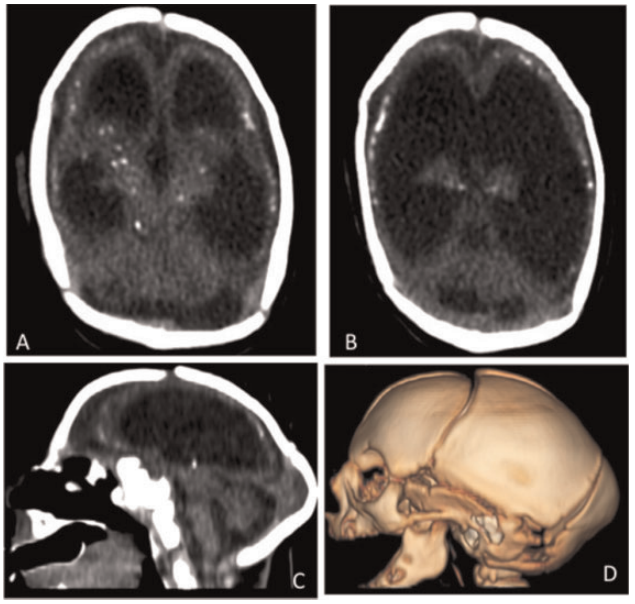

FIGURE 1. Brain CT scan: axial planes **(A, B)**, sagittal section **(C)**, and 3D reconstruction **(D)** shows: microcephaly **(C, D)**, with diffuse hypogyration **(A–C)**, multiple isolated punctate calcifications at the cortico/white matter junction, basal ganglia and thalami **(A)**, and band-like calcifications at periventricular white matter **(B)**, ventriculomegaly **(A–C)**, cerebellar and brainstem hypoplasia **(C)**, and a pointed occiput **(C, D).**

MATERIALS AND METHODS

This study was approved by the local internal review board under the number CAAE 52675616.0.0000.5269. Informed consent to perform the autopsy was obtained from the parents of the infant.

Real-time RT-qPCR assay for ZIKV was performed at delivery on maternal plasma, placenta samples, on cerebrospinal fluid (CSF), and urine samples of the neonate, as well as in tissues obtained at autopsy. ZIKV RNA detection was performed following total RNA extraction using TRIzol Reagent (ThermoFisher, Waltham, MA) according to the manufacturer's instructions. Maternal and neonatal body fluids or 100 mg of snap frozen autopsy tissues were homogenized in 1 mL of TRIzol Reagent to further chloroform RNA extraction. All samples tested presented RNA purity higher than 1.9 measured by 260/280 nm ratio (1000 Nanodrop, ThermoScientific). RT-PCR was performed with the 2× QuantiTect Probe RT-PCR kit (Qiagen, Valencia, CA) with the same primers and cycle times as previously described (1, 11). All assays were done in triplicates and fluorescence growth curves that cross the threshold within or below 38 cycles were considered positive.

A detailed analysis of the placenta and umbilical cord and a full postmortem examination were performed. Fresh samples from the brain, spleen, thymus, adrenal, heart, kidney, lung, liver, salivary glands, and gastrointestinal tract were taken to investigate the presence of ZIKV with PCR. Samples of all organs were fixed in 10% formalin and then processed for paraffin embedding. The brain, spinal cord and dorsal root ganglia were fixed in 10% formalin for 2 weeks. Formalin fixed brain was weighed and after gross examination, representative areas, including those with macroscopic lesions, were processed for paraffin embedding and 5-μm histological sections were stained with hematoxylin and eosin (H&E). From selected blocks of the cerebral hemispheres, brainstem, cerebellum, and spinal cord, 10-μm sections were stained with Luxol fast blue (LFB) for myelin.

From the leptomeninges and selected areas of the nervous tissue with histological lesions, immuno-histochemical reactions were performed, using the following monoclonal antibodies (Cell Marque, Sigma–Aldrich Co, Rocklin, CA) and dilutions: antiglial fibrillary acidic protein-GFAP-clone EP672y, (1:500), antiCD68 clone Kp-1 (1:1000), antiOlig2 clone 211F1.1 (1:200), and antiNeuN (Zeta Corporation, Arcadia, CA) Clone A100 (1:200). The immunohistochemical methods have been previously described (5).

ZIKV ISH studies were performed on formalin-fixed paraffin-embedded tissue sections of the brain, liver, kidney, spleen, heart, adrenal, using 2 commercial RNAscope Target Probes (Advanced Cell Diagnostics, Hayward, CA) catalog # 464531 and 463781 complementary to sequences 866-1763 and 1550-2456 of ZIKV genome, respectively, as cited previously (5).

FIGURE 2. (A) The infant showed arthrogryposis in all 4 limbs. **(B)** Inferior surface of the brain with shallow sulci and congested leptomeninges covered by purulent exudate. **(C)** Coronal sections showing severely dilated ventricles, reduced thickness of the cortex and white matter and flat deep gray nuclei. **(D)** Cerebellum covered by purulent exudate. **(E)** Sections of the brainstem showing that in the midbrain the aqueduct was not always visible and the pons and medulla were small.

RESULTS

Diagnosis of Zika Infection

At delivery, RT-qPCR assay of maternal plasma and placenta samples detected ZIKV RNA. Both maternal samples presented 3.5×10^5 viral RNA copies/mL. After birth only urine of the neonate was positive with 3.2×10^5 viral RNA copies/mL. Among the organs sampled at autopsy, ZIKV RNA was detected only in the brain, with 7.5×10^5 viral RNA copies/mg of tissue, indicating viral persistence.

Placenta

There was focal chronic villitis and villous immaturity, stromal fibrosis, fibromuscular hyperplasia of vessel walls, and chronic deciduitis. The umbilical cord was normal.

Autopsy

The infant weighed 5360 g, measured 60 cm and had arthrogryposis in all 4 limbs (Fig. 2A). The brain weighed 150 g (expected weight, 644 g [12]). Leptomeninges were congested and covered by purulent exudate. A catheter was in place in the lateral left ventricle. The brain showed a smooth surface with shallow sulci. On sectioning the ventricles were severely dilated, the ependymal surfaces were also covered by pus, the thickness of the cortex and white matter was reduced to 0.5 cm in some regions and the basal ganglia and thalami were flat. The hippocampi were not readily delineated. The cerebellum was covered by purulent exudate and sections of the brainstem showed that the aqueduct was not always visible, particularly at the upper level of the midbrain, and the pons and medulla were small. Macroscopic appearances are illustrated in Figure 2.

Microscopically there was acute exudative meningitis. The cerebral cortex was practically devoid of neurons in several areas and those present were disorganized. Immunostaining for NeuN confirmed neuronal loss with thin cortical mantle showing no neurons while regions with wider cortical mantle showing occasional nerve cells. There were disturbances of neuronal migration in the cerebral hemispheres including dyslamination and meningeal glioneuronal heterotopia. Fine or coarse calcification in various levels of the hemispheric parenchyma was also seen, in addition to severe gliosis. The ependyma showed multifocal erosions with granulations and a neutrophilic exudate. On LFB-stained sections, myelinated fibers were practically absent in hemispheric white matter, whereas deeper regions, posterior fossa structures, and the spinal cord, were myelinated. Oligodendrocytes stained with OLIG2 were very scarce in the hemisphere, while in the deeper regions they were more frequent. The shape of the hippocampus was recognized, although the dentate gyrus was not well formed. The loose appearance of the CA sectors seems to be due to lack of nerve cells. Histology of supratentorial structures is illustrated in Figure 3.

The cerebellum had no parenchymal lesion. In the midbrain, although the aqueduct appeared patent, it contained an inflammatory exudate and at proximal levels was elongated and narrow. There were occasional foci of calcification and extensive gliosis, particularly around the narrow aqueduct where microglial proliferation was prominent. The basis pontis and pyramids were small, but other brainstem structures were normal. There was inflammatory exudate at the fourth ventricle surface and its outlet.

The spinal cord was abnormally shaped due to a reduction in the size of the lateral cortico-spinal tracts, in addition to motor nerve cell loss, gliosis and small foci of calcification. The dorsal column was preserved and myelinated, as were the dorsal nerve roots, and ganglia. Microscopic findings in infratentorial and spinal structures are illustrated in Figure 4.

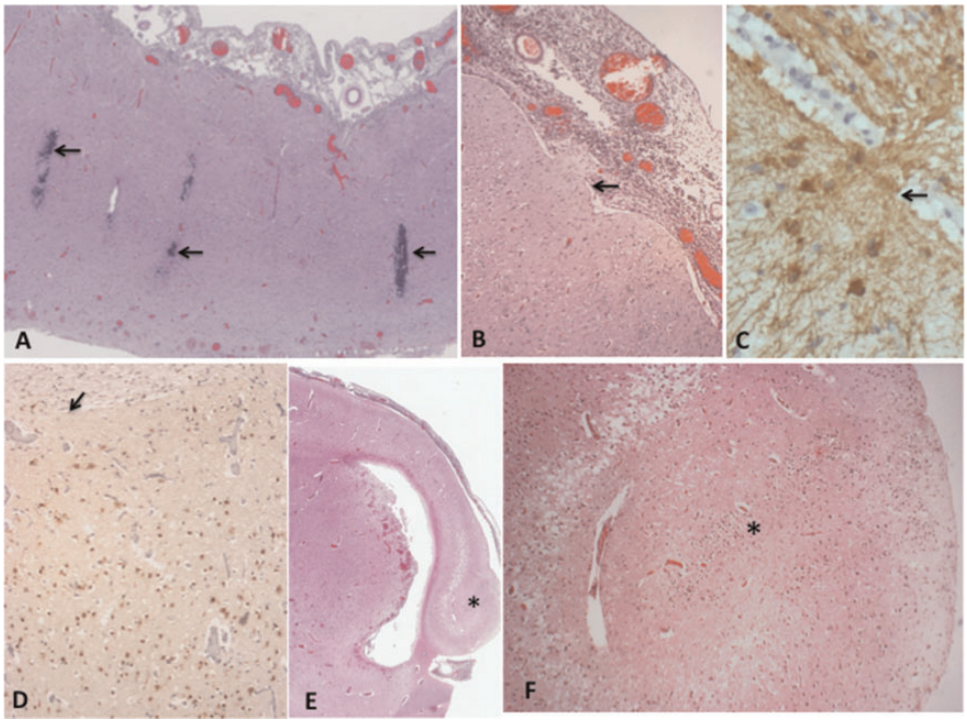

FIGURE 3. (A) The whole thickness of the hemisphere, showing various clusters of calcification (arrows). **(B)** Acute exudative meningitis. Disturbances of neuronal migration including dyslamination, meningeal glioneuronal heterotopia **(B–D,** arrows indicating where piamater is interrupted), and gliosis **(C)**. **(E)** The shape of the hippocampus (*) can be seen at the right of the temporal horn of the lateral ventricle. **(F)** The loose appearance of the CA sectors is seen, while the dentate gyrus is not well delineated (*). H&E, GFAP **(C)**, NeuN **(D).**

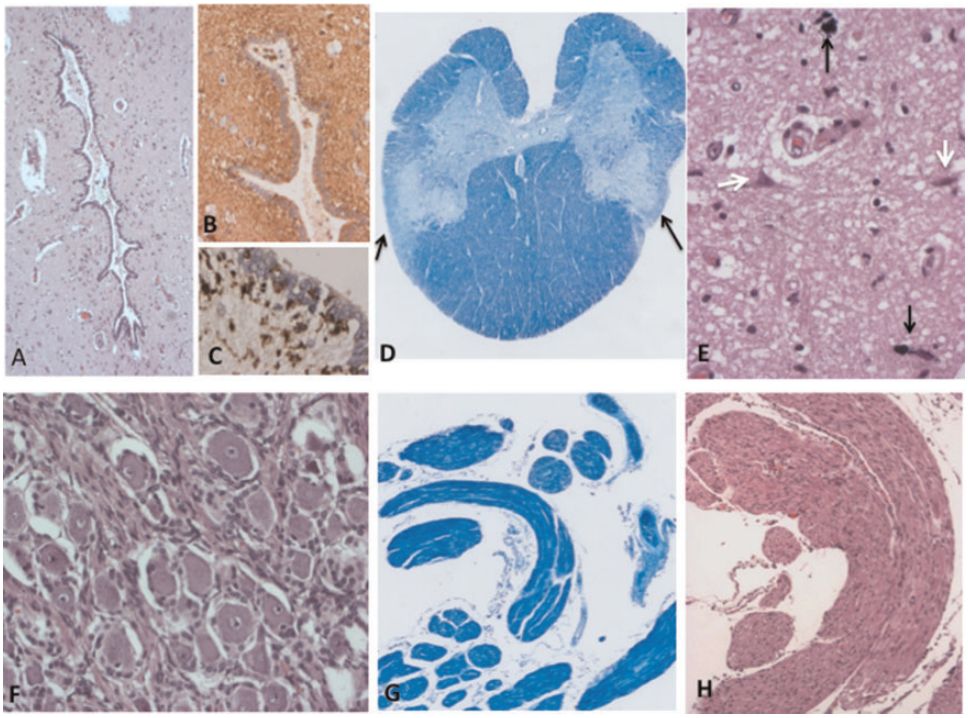

FIGURE 4. (A) Narrow aqueduct surrounded by gliosis **(B)** and microglial proliferation **(C)**. **(D)** Narrow spinal cord due to small lateral cortico-spinal tracts (arrows), while the dorsal column is normal and well myelinated. **(E)** Few shrunken motor nerve cells (white arrows) and small foci of calcification (black arrows) are observed in the anterior horn. The dorsal root ganglion is well populated of neurons **(F)** and the dorsal roots are normal **(G, H)**. H&E, GFAP **(B)**, CD68 **(C)**, LFB **(D, G).**

Lymphocytic infiltration was not observed in any segment of the brain and spinal cord. No cytoplasmic or nuclear inclusions, or parasites were seen. The pituitary gland showed foci of microcalcification.

In systemic tissues, in addition to generalized lymph node enlargement, there was acute tracheitis, focal erosion and mucoid material with neutrophils in the lumen, bronchopneumonia and changes consistent with phase II shock lung. The cardiac cavities were filled with leucocytes and fibrin. There was chronic esophagitis with focal parietal fibrosis permeating and dissociating the muscular layer.

The diaphragm showed focal fibrosis in the thoracic and abdominal aspects, associated with a mild mixed inflammatory interstitial process permeating the muscle bundles, some of which were very thin (neurogenic atrophy). There was moderate acute and chronic peritonitis and mesenteric lymphoid hyperplasia. The spleen had sinusoidal congestion of red pulp and mild depletion of white pulp; the liver showed microesteatosis and cholestasis.

Other lesions included acute tubular necrosis in the kidneys, mild chronic cystitis and fibrosis permeating the muscle bundles. Extramedullary hemopoiesis was present in kidneys and liver. The uterus and fallopian tubes had chronic and acute serositis. The cause of death was bacterial sepsis with meningitis, bronchopneumonia and focal abdominal infection. ISH results for ZIKV in all samples examined were negative.

DISCUSSION

In the case described here, ZIKV infection clinically occurred in the first trimester of gestation consistent with the magnitude and character of the cerebral lesions, observed both with the images and the pathological analysis. The first laboratory confirmation of infection was detection of viral RNA in the amniotic fluid at the end of the second trimester (24 weeks and 5 days). The neuropathological findings were comparably severe to those found in stillborn and neonates who died soon after birth but were infected in the beginning of gestation (3, 5, 6). The spinal cord changes are consistent with the arthrogryposis seen in this and in previously reported cases (5).

Bacterial meningitis in this case was attributed to infection of the ventricle peritoneal shunt, a major cause of morbidity and mortality in children with hydrocephalus requiring CSF shunts (13). Unexplained was the development of hydrocephalus after the fourth month of life. Since the aqueduct was focally narrow, we cannot exclude the possibility that gliosis and microglial proliferation may have contributed to its compression obstructing the CSF flow.

Many children born with ZIKV-related complications are alive, but their long-term developmental trajectory needs to be investigated. As observed in the present case, clinicians are now describing infants with exaggerated primitive reflexes, epilepsy, acquired hydrocephalus and microcephaly, neurodevelopmental delay, marked early hypertonia, extrapyramidal symptoms, gastrointestinal motility problems and respiratory complications (2, 7, 14). In addition, swallowing dysfunctions increase the risk for aspiration of liquid foods (8).

Viral persistence in maternal blood at the time of birth can be related to a failure of antiviral immunological clearance or the consequence of maternal reseeding from fetal infection (15). Viral persistence as indicated by maintenance of PCR positivity in postmortem tissue could be explained by a variety of mechanisms. Selective presence in brain and placental tissues could be the results of diminished immune surveillance in these regions (so called immunological privilege) (4). Experimental studies have proposed persistent or occult neurologic and lymphoid disease following clearance of peripheral virus in ZIKV-infected animals (9). The multiple potential explanations for why in our subject ZIKV was detected by PCR and not ISH, can be grouped under 4 broad categories: preservation, viral load, sampling and technological sensitivity. For PCR, frozen tissue was available for nucleic acid extraction. This avoids the vagaries of immersion fixation in formalin and would be expected in particular to provide better nucleic acid preservation. Additionally, viral load in our subject was orders of magnitude less than that detected during active infection. This made any detection highly dependent upon sampling. If equivalent size blocks of tissue were used in both PCR and ISH methods, it would be important to recognize that PCR results are the product of a highly amplified average while ISH is only selecting one tissue section out of hundreds for analysis. Finally, while ISH sensitively detects nucleic acids concentrated within individual cells, it lacks the exponential amplification afforded by PCR. Nevertheless, the fact that PCR was positive and ISH negative is important in considering the pathogenesis and therapeutic possibilities in late stage disease. As ZIKV load hovers at the limit of detection in this postnatal subject, it supports the concept favored in many other maternal/fetal infections that postnatal disease mostly reflects the aftermath of infection rather than continued immune mediated destruction.

The etiology of progressive disease after in utero infection is not clear. Findings in the current and other clinical studies suggest that active ZIKV replication is much diminished at late stages (inability to detect infected cells by ISH). This suggests several possibilities for the apparent later clinical progression. One possibility would be that immune reactions to ZIKV infection might cross-react with brain-specific proteins, causing additional neurological damage (16). Alternatively, exacerbation of neurological disease could be a pseudoprogression resulting from unmasking of the extent of neurological damage with development. Examination of additional cases should help better delineate the pathogenesis.

REFERENCES

1. Brasil P, Pereira JP, Moreira ME, et al. Zika virus infection in pregnant women in Rio de Janeiro. New Engl J Med 2016;375:2321–34
2. Moore CA, Staples JE, Dobyns WB, et al. Characterizing the pattern of anomalies in congenital zika syndrome for pediatric clinicians. JAMA Pediatr 2017;171:288–95
3. Sousa AQ, Cavalcante DIM, Franco LM, et al. Postmortem findings for 7 neonates with congenital Zika virus infection. Emerg Infect Dis 2017;23: 1164–7
4. Bhatnagar J, Rabeneck DB, Martines RB, et al. Zika virus RNA replication and persistence in brain and placental tissue. Emerg Infect Dis 2017; 23:405–14

5. Chimelli L, Melo ASO, Avvad-Portari E, et al. The spectrum of neuropathological changes associated with congenital Zika virus infection. Acta Neuropathol 2017;133:983–99
6. Schwartz DA. Autopsy and postmortem studies are concordant: pathology of Zika virus infection is neurotropic in fetuses and infants with microcephaly following transplacental transmission. Arch Pathol Lab Med 2017;141:68–72
7. Kapogiannis BG, Chakhtoura N, Hazra R, et al. Bridging knowledge gaps to understand how Zika virus exposure and infection affect child development. JAMA Pediatr 2017;171:478–85
8. Leal MC, van der Linden V, Bezerra TP, et al. Characteristics of dysphagia in infants with microcephaly caused by congenital Zika virus infection, Brazil, 2015. Emerg Infect Dis 2017;23:1253–9
9. Aid M, Abbink P, Larocca RA, et al. Zika virus persistence in the central nervous system and lymph nodes of Rhesus monkeys. Cell 2017;169: 610–20
10. Snijders RJ, Nicolaides KH. Fetal biometry at 14–40 weeks' gestation. Ultrasound Obstet Gynecol 1994;4:34–48
11. Lanciotti RS, Kosoy OL, Laven JJ, et al. Genetic and serologic properties of Zika virus associated with an epidemic, Yap State, Micronesia, 2007. Emerging Infect Dis 2008;14:1232–9
12. Sieber JR, Perinatal, fetal and embryonic autopsy. In: Gilbert-Barness E, ed. Potter's Pathology of the Fetus, Infant and Child. 2nd ed. Philadelphia, PA: Mosby-Elsevier 2007:695–739
13. Ochieng' N, Okechi H, Ferson S, et al. Bacteria causing ventriculoperitoneal shunt infections in a Kenyan population. J Neurosurg Pediatr 2015; 15:150–5
14. Moura da Silva AA, Ganz JS, Sousa PD, et al. Early growth and neurologic outcomes of infants with probable congenital Zika virus syndrome. Emerg Infect Dis 2016;22:1953–6
15. Driggers RW, Ho C-Y, Korhonen EM, et al. Zika virus infection with prolonged maternal viremia and fetal brain abnormalities. N Engl J Med 2016;374:2142–51
16. Lucchese G, Kanduc D. Zika virus and autoimmunity: from microcephaly to Guillain-Barré syndrome, and beyond. Autoimmun Rev 2016;15: 801–8